Pyromellitic Diimide Based Bipolar Molecule for Total Organic Symmetric Redox Flow Battery

Gabriel Sikukuu Nambafu [a], Ernest Pahuyo Delmo [a], Usman Bin Shahid [a], Cheng Zhang [b,c], Qing Chen [b,c], Tianshou Zhao [b,c], Ping Gao [a,c], Khalil Amine [d,e,*], Minhua Shao [a,c,*]

[a] Department of Chemical and Biological Engineering, The Hong Kong University of Science and Technology, Clear Water Bay, Kowloon, Hong Kong

[b] Department of Mechanical and Aerospace Engineering, The Hong Kong University of Science and Technology, Clear Water Bay, Kowloon, Hong Kong

[c] Energy Institute, The Hong Kong University of Science and Technology, Clear Water Bay, Kowloon, Hong Kong

[d] Chemical Sciences and Engineering Division, Argonne National Laboratory, 9700 South Cass Avenue, Lemont, II, 60439, United States

[e] Materials Science and Engineering, Stanford University, Stanford, 94305, United States

*Corresponding authors: amine@anl.gov; kemshao@ust.hk

Abstract

Non-aqueous redox flow batteries based on total organic electrolytes, consisting of earth-abundant elements, i.e., C, H, N, O, are regarded as a promising technology for sustainable and large-scale energy storage. In particular, bipolar redox-active organic materials (BROMs) are distinctly fascinating as electroactive species because they have multiple oxidation states and can undergo multiple redox processes. By virtue of this unique characteristic, BROMs can be utilized as both anolyte and catholyte in symmetric flow batteries, consequently, helping alleviate cross-contamination issues. Herein we report an all-organic symmetric redox flow battery based on diimide molecule as a bipolar electroactive material. The potential interval between the cathodic peak and the inner and outer anodic peaks led to a promising cell voltage of 2.22 V. The symmetric battery can be operated at a current density of 20 mA cm^{-2}, with a coulombic efficiency of 90 % for over 100 cycles. This work proposes an alternative approach to designing multi-electron organic redox active materials to facilitate the advancement of high-density symmetric flow batteries.

Keywords: Pyromellitic diimide; electroactive materials; bipolar organic molecules; symmetric non-aqueous redox flow battery

Introduction

Climate change, environmental concerns, and increasing energy demands have propelled global energy transformation towards renewable energy technologies, such as wind and solar energy systems [1-5]. However, the large-scale distribution and application of these energy systems have been hindered by their sporadic and unreliable nature [6,7]. Redox flow batteries (RFBs) are scalable and allow decoupling of power and energy capacity, a unique feature that makes them a promising large-scale energy storage device to regulate and support the intermittent renewable energy sources [8-12].

In recent years, there has been a massive development in RFBs by using organic redox-active materials [13]. Properties such as large theoretical capacities, abundance in nature, cost-effectiveness, diverse and tuneable structures make them preferable compared to their inorganic counterparts [14-16]. Nonetheless, the narrow electrochemical stability window of water limits the cell voltage and energy density of aqueous organic RFBs, thus hindering their advancement and development [17]. On the other hand, non-aqueous organic RFBs utilizing organic solvents with wider potential windows facilitate a higher energy density. Additionally, they offer a broader working temperature ranges and provide alternative solvents to the non-polar/hydrophobic redox-active materials permitting high solubility [17-20]. Asymmetric non-aqueous RFBs employing different organic molecules as positive and negative electrolytes have already been investigated. However, their commercialization has been hindered by several issues, including, but not limited to, low cycle life, low energy density, etc. [21,22] Cross-mixing of the positive and negative electrolytes during cycling prompting capacity losses and self-discharge has been the predominant challenge. Various strategies have been deployed to address this setback, such as (1) employing the same metal ion with different oxidation states as catholyte and anolyte as in all vanadium symmetric flow battery [23]; (2) catholyte-anolyte mixture; entails physically mixing the catholyte and anolyte before utilizing them as electrolyte [24]; (3) employing a single redox active material with bifunctional properties and capability as both catholyte and anolyte in RFBs [25].

Bipolar redox-active organic molecules (BROMs) are emerging as suitable candidates for the next generation of electroactive energy storage materials for RFBs [26]. This is by virtue of their multiple redox states; hence they can be deployed as both positive and negative materials in the battery. These materials are applied in symmetric battery concept, which is simple to design and helps evade cross-contamination issues [26]. Several inorganics, organic and organometallic bipolar redox-active molecules have already been investigated in symmetric RFBs [27-36]. However, various challenges such as low solubility and stability have been identified. Therefore, there is a need to design ideal BROMs to facilitate and accelerate the development of high-performance symmetric organic RFBs.

Motivated by recent developments in symmetric organic RFBs, herein we design, synthesize and evaluate pyromellitic diimide-2,2,6,6-tetramethylpiperidine 1-Oxyl (PDI-TEMPO) molecule as a bipolar electroactive material in a symmetric non-aqueous flow battery. Pyromellitic dianhydride and TEMPO are fused together to form a combi molecule consisting of one PDI moiety and two TEMPO moieties. This design uses a simple one-step synthesis route utilizing low-cost and easily available precursors. The combi molecule displayed three redox couples at half potentials of -1.83 V, -1.14 V and 0.39 V vs Ag/Ag^+ in tetrabutylammonium hexafluorophosphate / dimethylformamide ($TBAPF_6$/DMF) supporting electrolyte and -1.72 V, -1.17 V and 0.45 V vs Ag/Ag^+ in tetrabutylammonium hexafluorophosphate / acetonitrile ($TBAPF_6$/ACN) supporting electrolyte. This resulted to a cell voltage of up to ~2.22 V. Battery cycling tests demonstrated 100 consecutive charge/discharge cycles with a coulombic efficiency of around 90%. Therefore, this work provides a pathway to design bifunctional multi-electron redox molecules which is a key concept in developing a long cycle life and a high energy density redox flow battery.

Chemicals and Materials

Pyromellitic dianhydride ($C_{10}H_2O_6$, 99%, Aladdin, China), 4-Amino-2,2,6,6-tetramethylpiperidine 1-Oxyl ($C_9H_{19}N_2O$, 97%, Aladdin, China), Glacial acetic acid (AcOH / CH_3CO_2H, ≥ 99.0% pure, Sigma Aldrich), Tetrabutylammonium hexafluorophosphate ($TBAPF_6$ / $C_{16}H_{36}N{\cdot}PF_6$, ≥ 98% pure Aladdin, China), Dichloromethane (CH_2Cl_2, 99.8%, Sigma Aldrich), Dimethylformamide (DMF, 99.8%, Sigma Aldrich), Acetonitrile (ACN, 99.8%, Sigma Aldrich), were purchased from the named suppliers and used as received without any purification. Argon gas was used for the protection of all oxygen-sensitive reactions.

Synthesis method

The PDI-TEMPO molecule was synthesized by modifying the existing procedures described in previous literatures [37-39]. Pyromellitic dianhydride (0.65g, 3 mM) and 4-Amino-2,2,6,6-tetramethylpiperidine 1-Oxyl (0.1g, 6 mM) were dissolved in 0.1 M acetic acid (40 mL) in a 50 ml three neck round-bottomed flask equipped with a magnetic stirrer. Upon complete dissolution of the materials, the flask was equipped with a condenser, and the reaction mixture was refluxed at 120°C for 24 hrs. Thereafter, the reaction mixture was cooled to room temperature, and the resulting precipitate was collected by filtration. The residue was then collected and washed with dichloromethane for three successive times. The brown powder was collected as product (Yield = 92%). The synthesis pathway of the PDI-TEMPO molecule is as shown in Figure S1. The resulting product was characterised by mass spectrometry (GCT premier CAB048 mass spectrometer), Time-of-Flight Secondary Ion Mass Spectrometry TOF SIMS V (ION-TOF GmbH) equipped with Bi cluster, Cs and C60 primary ion sources and ^{1}H NMR spectra was recorded on a Varian Mercury 300 MHz High Resolution Spectrometer.

Solubility test

The solubilities of pyromellitic dianhydride and PDI-TEMPO combined molecule in 0.1M $TBAPF_6$/ACN or DMF were evaluated using UV-Vis spectroscopy (PerkinElmer, Lambda 20). The standard calibration curves were prepared using absorbance units of various pyromellitic dianhydride and PDI-TEMPO in $TBAPF_6$/ACN or DMF standard solutions at the peak wavelengths of 250 nm and 319 nm respectively. Thereafter, saturated solutions were prepared and diluted to obtain solutions whose UV–Vis absorbance units at specific wavelengths were used to determine the molecule's solubility based on the standard calibration curve.

Electrochemical Characterisations

The Cyclic Voltammetry (CV) and Linear Sweep Voltammetry (LSV) studies were carried out in a three-electrode electrochemical cell, with Ag/Ag^+ non-aqueous reference electrode at room temperature. A glassy carbon disk (5 mm diameter), and a platinum wire were employed as working and counter electrodes, respectively. The working electrode was polished on grit paper using Al_2O_3 suspension, ultrasonically cleaned with deionized water, and dried before use. The CV studies were carried out at a potential range of -2.5 V to 1.0 V at a scan rate of 50 mv s^{-1}. For the scan rate dependence measurements, different scan rates ranging from 50 mV s^{-1} to 500 mV s^{-1} were used. The LSV measurements were conducted with a rotating disc electrode at speeds ranging from 0 rpm to 2000 rpm with a scan rate of 5 mV s^{-1} from -3.0 V to 1.0 V. The electrode was rotated using Pine research modulated speed rotator (AFMSRCE 2252). Both CV and LSV studies were performed using an electrochemical working station controlled by a potentiostat from CH instruments (CHI 760 or 627e) under the continuous flow of argon gas into the cell to provide an inert atmosphere.

Cell fabrication

The flow battery was assembled using a cell stack, two storage tanks and a peristaltic pump. The cell stack tooling was fabricated by Shanghai SHIMATOYO Electronics Co., Ltd (China) with electrode and membrane-active area of 4 cm^2 and interdigitated flow field (IFF) design. Anion exchange membrane (FAB-PK-130) and graphite felt from Fuel Cell Store, USA (Figure S2) were employed as separator and electrode, respectively. Both the electrode and membrane were cut into suitable sizes and used as received without any prior treatment. A solution of PDI-TEMPO in $TBAPF_6$/ACN or DMF was prepared as the electrolyte and utilized as both the catholyte and anolyte. The electrolytes were circulated between the catholyte and anolyte storage tanks and cell stack by a single peristaltic pump (Longer Pump WT600-2J). The battery cycling test was done using the Neware battery testing system, and the data was recorded and stored in a computer. The charging and discharging process were conducted at different current densities, and cut-off voltage ranges. All measurements were carried out at room temperature.

Results and Discussion

Synthesis of imide

The PDI-TEMPO combi molecule was synthesized via a one-pot synthesis method using pyromellitic dianhydride and 4-amino TEMPO as basic materials. When pyromellitic dianhydride (acid anhydride) is mixed with 4-amino TEMPO (amine), in glacial acetic acid as solvent, the resulting product is an amic acid. This reaction pathway is only feasible at room temperature. However, conversion of amic acid to yield an imide is a very slow reaction at room temperature and can take a very long time to eventuate. Therefore, heating was essential to ensure a high rate of reaction to form the desired product as shown by schematic illustration in Figure S1. However, acetic acid has a low boiling point of 118°C and evaporates when the solution is heated to 120 °C, thus preventing the complete reaction of the reactants. Thus, heating under reflux was ideal to address this challenge [40]. The synthesis pathway of the target product from the precursors is shown in Figure 1 below. This product was obtained in high yield (92%). Mass spectra display molecular ion peaks at *m/z* values correlating with the molar mass of PDI-TEMPO molecule in both high-resolution mass spectrometry analysis and TOF-SIMS analysis as shown in Figure S3 and S4 respectively. Additionally, ^{1}H NMR spectra display proton signals corresponding to hydrogen atoms present in the target product as shown in Figure S5.

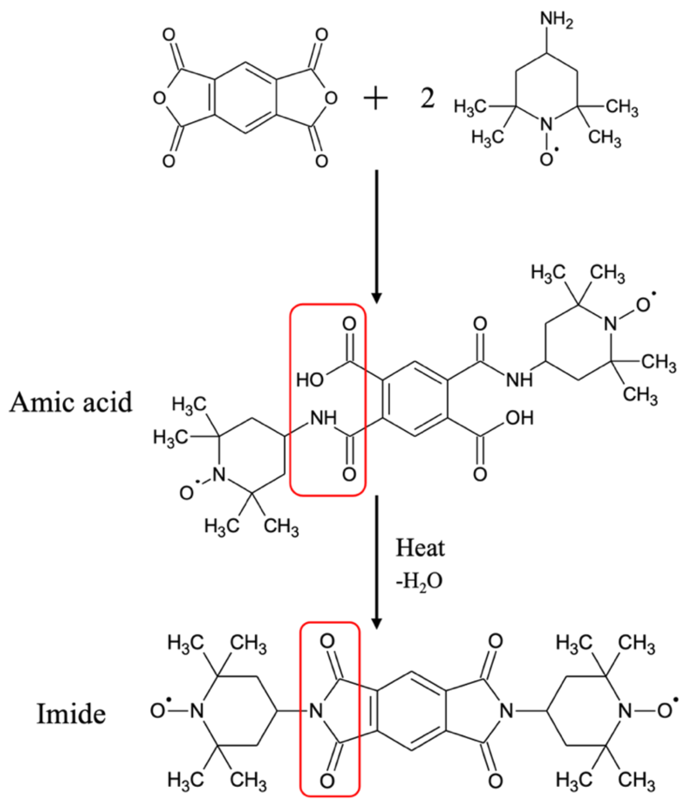

Figure 1. Synthesis pathway of PDI-TEMPO from pyromellitic dianhydride and amino-TEMPO.

Electrochemical Properties

The electrochemical properties of the redox-active materials were evaluated accordingly. CVs were employed to determine the redox states and redox potentials, whereas RDE studies were used to determine the diffusion coefficients and rate constants of the electroactive species. First, the electrochemical properties of pyromellitic dianhydride were evaluated. CV analysis of pyromellitic anhydride in 0.1 M $TBAPF_6$/ACN displayed two redox couples with half potentials of -1.46 V and - 0.83 V vs Ag/Ag^+ reference electrode, respectively, as shown in Figure 2a. The two redox couples are associated with two sequential one-electron transfer redox processes of the molecule. The CV of amino TEMPO as displayed in Figure 2b, exhibited one redox couple at a half potential of 0.52 V vs Ag/Ag^+. This leads to a potential interval of 1.98 V and 1.35 V with consideration of pyromellitic dianhydride (outer peak-I and inner peak-II) and amino TEMPO as anolyte and catholyte, respectively. Consequently, CV analysis of PDI-TEMPO bipolar molecule in 0.1 M $TBAPF_6$/ACN displayed three expected electrochemically reversible redox events with the half redox potentials at -1.72 V, - 1.17 V and 0.45 V as shown in Figure 2c. The two redox couples at the lower potential zone and one redox couple at the higher potential zone are associated with the PDI and TEMPO moiety, respectively. This resulted in a cell voltage of 1.62 V and 2.17 V between TEMPO/TEMPO + redox couple and the inner and outer redox couples (one and two-electron redox reactions) of the PDI moiety, respectively. The redox mechanism for the combined molecule during the charge and discharge process is shown in Figure 2e. The PDI moiety undergoes two sequential one-electron transfer redox reactions based on oxidation and reduction of the two carbonyl functional groups as shown in Figure 2e and Figure S6. This is in agreement with already reported computational studies on the molecule [38]. On the other hand, TEMPO undergoes one-electron transfer redox process, as it involves the conversion of the nitroxide radical to oxoammonium cation and vice versa during the charge and discharge process. Two TEMPO moieties in the molecule structure provided a balance of electrons transferred for the anolyte and catholyte; two electron each for both moieties. In comparison with individual molecules, CV analysis of PDI-TEMPO demonstrated improved cell voltage, majorly, as a consequence of negative redox potentials shifts associated with the two redox processes for the PDI moiety. Negative redox potential shifts of 0.26 V and 0.34 V were observed for the first and second peaks respectively.

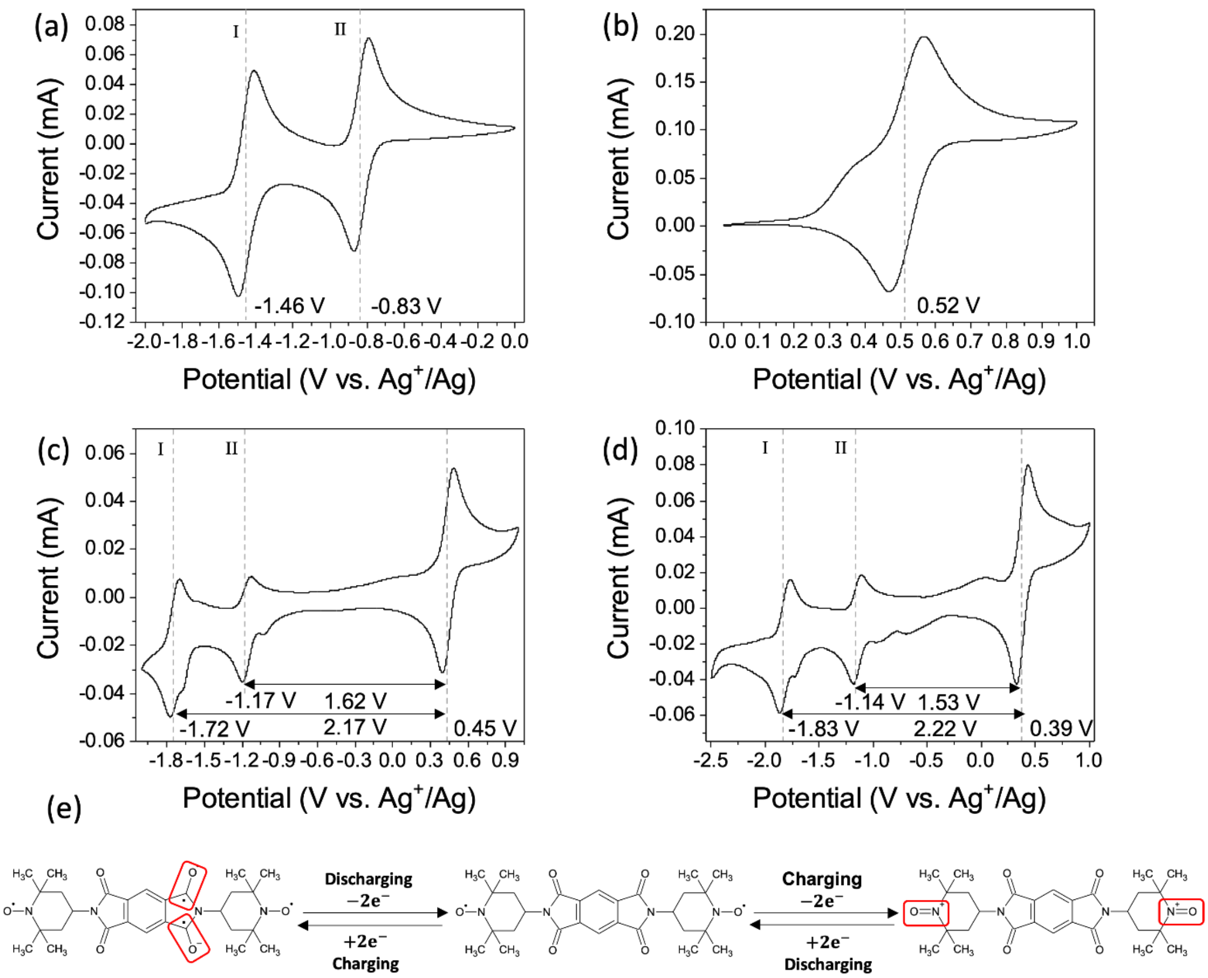

Figure 2. Cyclic voltammograms at a scan rate of 50 mV s^{-1} in 0.1M $TBAPF_6$/ACN as supporting electrolyte for (a) pyromellitic dianhydride, (b) 4-amino TEMPO , (c) PDI-TEMPO in 0.1M $TBAPF_6$/ACN, (d) PDI-TEMPO in 0.1M $TBAPF_6$/DMF as supporting electrolytes, (e) redox mechanism of PDI-TEMPO during charge and discharge process.

Supplementarily, the electrochemical properties of the bipolar molecule in DMF as the supporting electrolyte was also evaluated. CV analysis of PDI-TEMPO in $TBAPF_6$/DMF displayed redox couple at half potentials of -1.83 V, -1.14 V, and 0.39 V vs. Ag/Ag^+ as shown in Figure 2d. This led to a theoretical cell voltage of 1.53 V and 2.22 V for a symmetric battery based on the bipolar molecule. The different properties of the supporting electrolytes employed i.e. ACN and DMF resulted in differences in the half potentials of the redox couples observed. Moreover, CV tests confirmed the high stability of the bipolar molecule, as the voltammograms overlap with each other for over 100 cycles as shown in Figure 3a. Scan-rate-dependent CV studies exhibit an increase in peak current with increase in scanning rates (Figure 3b). Accordingly, the plots of peak current versus the square root of the scan rate were obtained as shown in Figure 3c and 3d for PDI and TEMPO moiety, respectively. A linear relationship between the peak currents and the square root of the scan rates confirms a diffusion-controlled behaviour of the redox processes. A diffusion coefficient of 1.639×10^{-6} cm^2 s^{-1}, 1.095×10^{-6} cm^2 s^{-1} (peak I and II respectively) for PDI moiety and 2.322×10^{-6} cm^2 s^{-1} for TEMPO moiety in $TBAPF_6$/ACN were calculated according to the Randles-Sevcik equation [27,28]. A comparison of the diffusion coefficients for pyromellitic dianhydride, amino TEMPO and PDI-TEMPO combi molecule calculated from plots shown in Figure S7 and S8 is shown in Table S1. The diffusion coefficients of the combi molecule were smaller than those of individual molecule due to its larger size. Mass transport in the electrolyte solution is usually dependent on various factors such as shape and size of the redox-active molecule, viscosity of the supporting electrolyte, temperature etc. [41,42]. Fundamentally, the diffusion coefficients obtained are in the same magnitudes as those of other organic molecules already investigated as active materials in RFBs, thus confirming the potential of PDI-TEMPO as an electroactive material for RFB [26,31].

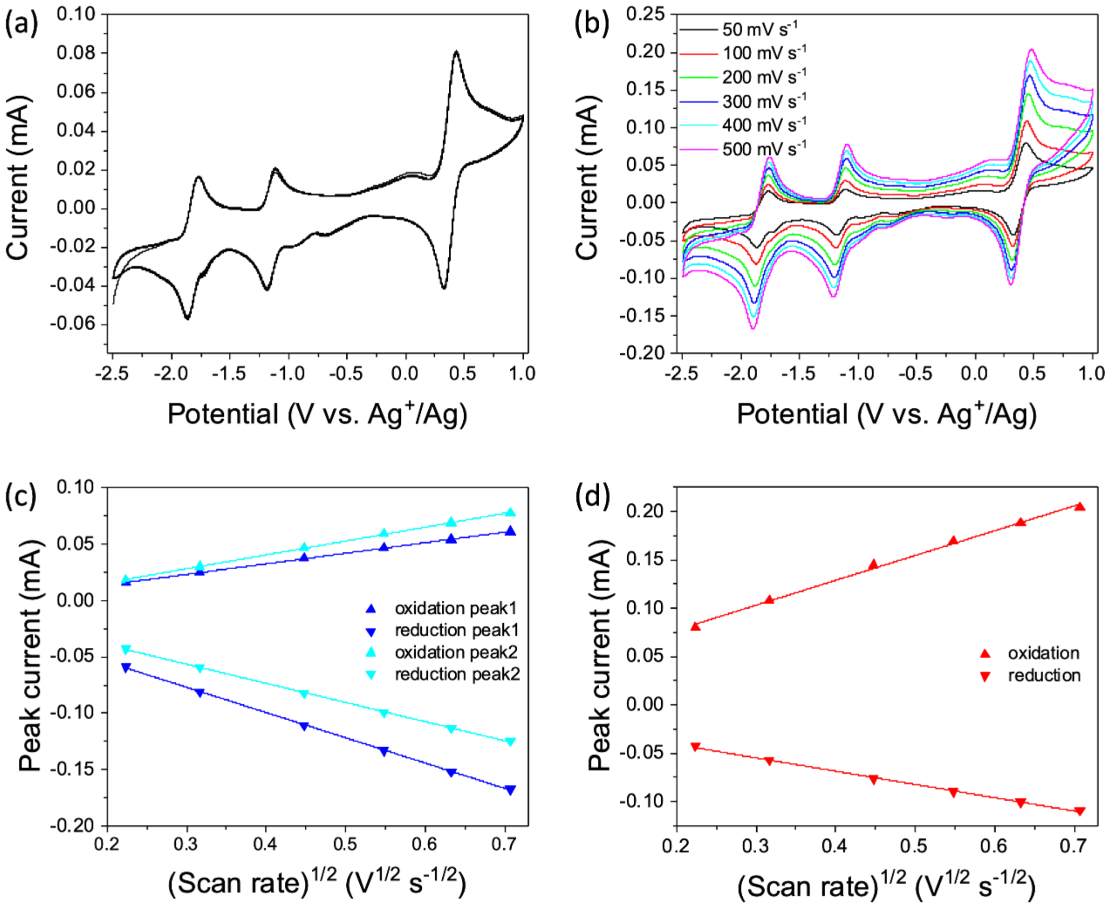

Figure 3. Cyclic voltammograms of 2 mM PDI-TEMPO in 0.1M $TBAPF_6$/DMF as supporting electrolyte (a) for 100 cycles at scan rate of 50 mV s^{-1}, (b) at different scan rates from 50 – 500 mV s^{-1}, and plot of peak current versus square root of scan rate (c) for PDI moiety, (d) TEMPO moiety.

Additionally, RDE study was also applied in determining the diffusion coefficient (D) of PDI-TEMPO in 0.1M $TBAPF_6$/DMF supporting electrolyte in conformity with the Levich equation stated below [43],

$$slope\ of\ the\ levich\ plot = 0.620\, nFAC_0\, D^{\frac{2}{3}} \upsilon^{-\frac{1}{6}},$$

where n = number of electrons transferred, Faraday's constant F = 96,485 C mol^{-1}, surface area A = 0.196 cm^2, the kinematic viscosity of DMF solutions $v = 8.37\times10^{-7}$ m^2 s^{-1} at 298.3 K and the C_0 = concentration of the redox-active material. Diffusion coefficients of 4.836×10^{-5} cm^2 s^{-1}, 3.515×10^{-5} cm^2 s^{-1} and 3.403×10^{-6} cm^2 s^{-1} were obtained for PDI (peak 1 and 2) and TEMPO moieties respectively, calculation done based on Figure S9. Furthermore, based on the plots of log i_k versus the overpotential and Tafel plots shown in Figure S10, the electron transfer rate constants were calculated using the equation below:

$$i = nFAk_oC$$

Where n, F, A and C are as defined in the Levich equation above, i is the current. k_o were calculated to be 5.063×10^{-3} cm s^{-1} and 1.826×10^{-3} cm s^{-1} for PDI and TEMPO moieties respectively, which are comparable to their counterparts already studied as active materials in organic non-aqueous flow batteries [24,26,29].

Battery tests

Essentially, the solubility and pre-cycling stability of PDI-TEMPO molecule were first investigated. The solubility of the redox-active materials was evaluated using UV-Vis spectroscopy, whereas the pre-cycling stability study of the molecule was investigated using both UV-Vis spectroscopy and CV. The solubility of PDI-TEMPO in 0.1 M $TBAPF_6$/ACN was 1.3 M as shown in Figure S11. In consideration, the resulting energy densities were 37.63 and 75.60 WhL^{-1} taking into account the inner redox couple (one electron) and both inner and outer redox couples (two electrons transfer) of the PDI moiety, respectively. Pyromellitic dianhydride demonstrated a solubility of 0.5 M in 0.1 M $TBAPF_6$/ACN as shown in Figure S12, which is lower than the solubility of the combined molecule. The improved solubility of the combined molecule was probably effectuated by the introduction of TEMPO moieties. TEMPO has demonstrated high solubility (>5M) in $TBAPF_6$/ACN [44,45]. PDI-TEMPO demonstrated a lower solubility of 0.2 M in 0.1 M TBAPF6/DMF (Figure S13), which leads to an energy density of 11.90 WhL^{-1}. CV analysis and UV-Vis spectra reveal that the molecule remained stable, and no degradation was observed when kept in the supporting electrolyte for 14 consecutive days, as shown in Figure 4.

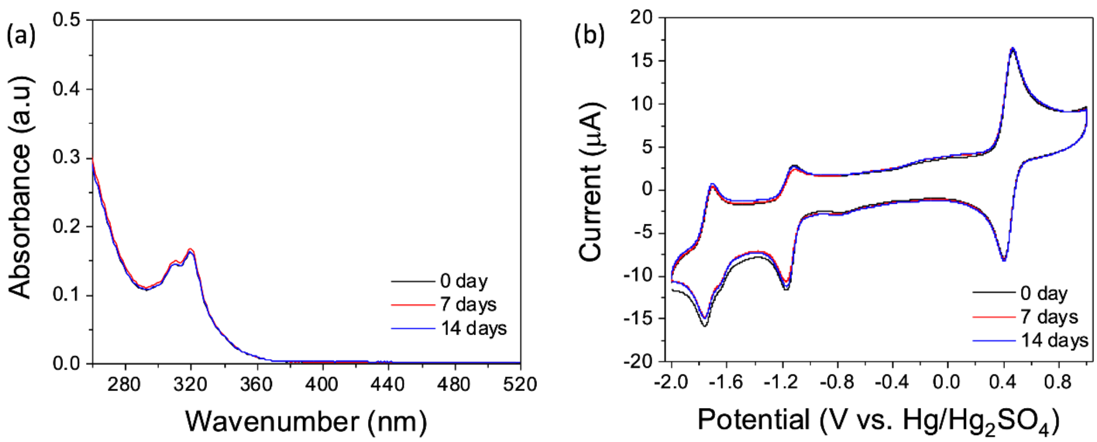

Figure 4. Stability analysis of 0.04 mM PDI-TEMPO stored in 0.1M $TBAPF_6$/ACN for 14 days (a) UV-Vis spectra (b) cyclic voltammograms at different time intervals.

Furthermore, the investigation of the PDI-TEMPO molecule as a bipolar redox-active molecule for application in RFB was done using a flow battery setup. A charge/discharge cut-off voltage range of 0.18 V – 2.4 V was utilized during the battery testing. PDI-TEMPO molecule exhibits redox properties in both DMF and ACN supporting electrolytes as shown in previous CV studies. However, ACN as the supporting electrolyte demonstrated better performance i.e. material utilization (Figure 5a), solubility and energy density in comparison to DMF supporting electrolyte. For instance, the flow battery test displayed a better capacity utilisation of ∼80% in ACN against ∼30% in DMF as shown in Figure 5a (theoretical capacity = 0.804 mAh). Also, a coulombic efficiency (CE)≈80% and voltage efficiency (VE)≈70% were achieved when utilising ACN solvent, whereas CE≈95% and VE≈60% were attained when employing DMF solvent during battery cycling as shown in Figure S14a. This is on account of the different properties of the two solvents/supporting electrolytes in terms of ionic conductivity, viscosity, density, dielectric constant, permittivity etc. [46]. Furthermore, system integration factors i.e. incompatibilities with cell components such as active materials, membrane, electrode and supporting ions may also have contributed to the low capacity utilisation in DMF solvent [19,46-49]. Battery cycling performances were also evaluated at different current densities. Representative charge and discharge curves during cycling are shown in Figure S14b. There was a rise in CE with increase in current density (Figure S14c) due to the reduction of charge/discharge period, hence less time for CE loss caused by capacity-related and non-capacity-related processes [31,49]. However, a decline in voltage efficiency was observed (Figure S14c), which was presumably caused by restricted ion conductivity in the electrolyte [31]. Moreover, cycling of PDI-TEMPO at a high concentration of 0.5 M and current density of 20 mA cm^{-2} demonstrated a promising result. Battery test displayed over 100 consecutive charge/discharge cycles with a columbic efficiency (CE) of 90 %, and average capacity retention of 99.4 % per cycle (Figure 5b). On the other hand, asymmetric flow battery based on pyromellitic dianhydride as negative material and amino-TEMPO as positive material exhibited over 10 charge and discharge cycles with coulombic efficiency of <80% and average capacity retention of 95% per cycle as shown in Figure S15. The better performance of applying the PDI-TEMPO can be due to the alleviation of cross-contamination issues in a symmetric flow battery setup. Besides, combining the molecules limits possibility of decomposition reactions by replacing the N-H (in diimides) adjacent to C=O (vulnerable to side reactions) with N-R (R=TEMPO), thus providing steric hindrance [50,51].

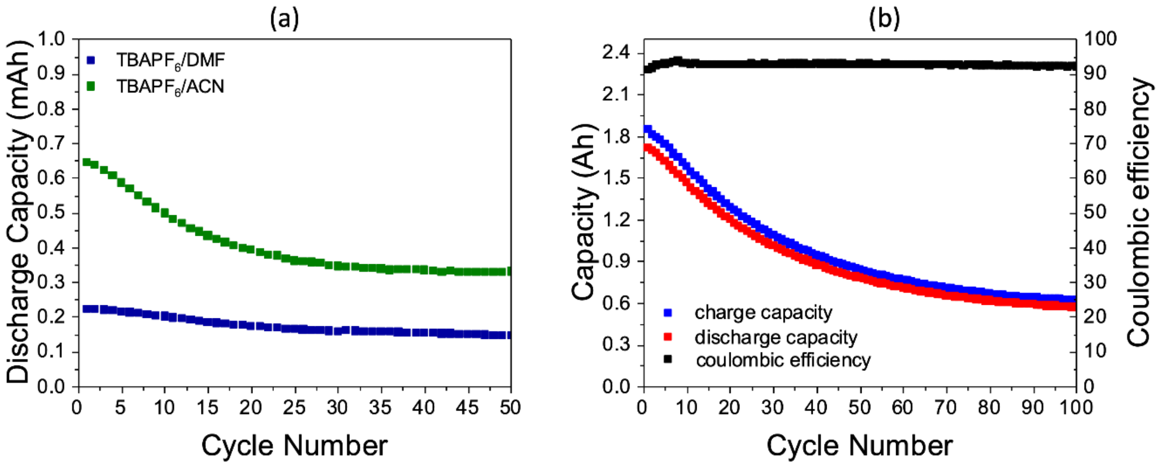

Figure 5. Battery cycling performance of (a) 1 mM PDI-TEMPO molecule in different supporting electrolytes at current density of 1 mA cm^{-2}, (b) 0.5 M PDI-TEMPO molecule in $TBAPF_6$/ACN at current density of 20 mA cm^{-2}.

Capacity fade during cycling is the major issue in this battery chemistry, similar to most organic battery chemistries [52]. Therefore, to understand the causes of capacity loss, fresh and spent electrolytes were examined by UV-Vis, CV and NMR. Analysis of catholyte displays negligible shifts in redox peaks as shown by UV-Vis spectra and CV results in Figure S16a& b, respectively. The redox peaks associated with all the three redox couples are present and peak potentials remain unchanged as seen in CVs. Besides, UV-Vis spectra display no shifts in the peak's wavelength. On the other hand, UV-Vis spectra of the anolyte display shift in peak wavelength as shown in Figure S16c. In addition, the CV result shows the disappearance of the redox peaks of the redox couple associated with the PDI moiety (Figure S16d). Moreover, CV studies of both electrolytes indicate appearance of an additional anodic peak at high potential zone with potential of 0.805 V vs. Ag^+/Ag. NMR spectra display emergence of a new single peak associated with -OH protons at $\delta = 2.0$ ppm as shown in Figure S17. The new peak sticks out more in spectrum of the spent anolyte in comparison to the spent catholyte spectrum. Based on the above results, the decomposition/ degradation of the PDI-TEMPO redox active molecule, more so the PDI moiety is probably the cause of capacity decay in this battery system. The faster capacity fade in ACN (0.6% per cycle) in comparison to DMF (0.2% per cycle) as exhibited in Figure 5a is believed to be caused by side reactions with acetonitrile [53]. The side reaction occurs via proton extraction at the $-CH_3$ group or protonation as shown in the proposed degradation mechanism in Figure S18 [53-55]. Predominantly, decomposition of the redox-active materials and side reactions is one of the major causes of capacity loss in organic-based RFBs. Advanced studies and investigation of the decomposition mechanisms are thus necessary to solve this challenge.

In comparison with other reported symmetric non-aqueous redox flow batteries [51], this work demonstrated the following merits. (1) PDI-TEMPO was synthesized in a high yield (92%) from commercially available materials via a simple one-step/one-pot method. (2) A symmetric RFB employing PDI-TEMPO as an active material demonstrated a cell voltage of 2.22 V, which is higher than most reported work. (3) It utilizes a cheaper anion exchange membrane (in comparison to cation exchange membrane) which can lead to a low-cost RFB system. (4) The molecule demonstrated high solubility of 1.3 M, leading to a high energy density of 75.60 WhL^{-1}. Further comparison with other reported work is shown in Table 1. It is worth noting that static and H-cells have been frequently used in non-aqueous system evaluation in literature, which doesn't provide an ideal experimental conditions for a RFB, e.g. flow rate, viscosity, pressure etc. To sum up, stability seems to be a major problem in BROMs based RFB according to most reported works [56]. Therefore, more efforts need to be invested in diagnosing this major challenge in symmetric organic-based redox flow batteries. Future work on the PDI-TEMPO battery chemistry will focus on cell design and molecule/electrolyte modifications to facilitate performance improvement and optimization.

Table 1. Performance metrics of symmetric non-aqueous redox flow batteries

Redox active materials	**Synthesis steps**	**Separator/ membrane**	**Battery type**	**Current density ($mA\ cm^{-2}$)**	**Cell potential (V)**	**Energy density (WhL^{-1})**	**Cycles/ Capacity retention (%)**	**Ref.**
Me-TEG-DAAQ	4 steps	Proton exchange membrane	Static cell	2	1.8 & 2.7	49 & 122	100/*48%	[27]
Verdazyl bipolar radical	3 steps	Anion exchange membrane	Static cell	0.12	0.98	0.52	50/35%	[28]
FcMeAAQ	2 steps	Daramic porous membrane	Flow cell	2	1.42	-	100/*50%	[29]
Nitronyl nitroxide	4 steps	Anion exchange membrane	Static & flow cell	1-5	1.62	4.1	75/80 % 11/50%	[31]
PTIO	-	Daramic porous membrane	Flow cell	20	1.7	11.6	35/*50%	[32]
Oxo-verdazyl radical	3 steps	Anion exchange membrane	Flow cell	2.22	1.42	-	80/36%	[33]

Porphyrin based molecule	-	(Y-PVDF) ion-selective membrane	Static and flow cell	1-5	2.83	24.68	200/*96%	[34]
All-Fullerene based molecule	2 steps	Glass fiber separator	Static cell	10	1.31 & 1.70	80	100/*50%	[35]
Dianion croconate violet	3 steps	Celgard separator	Flow cell	2.4	1.82	-	10/10%	[36]
PDI-TEMPO	1 step	Anion exchange membrane	Flow cell	20	~2.22	~75.60	100/40%	This work

Me-TEG-DAAQ = 1,4-bis((2-(2-(2-methoxyethoxy) ethoxy) ethyl) amino) anthracene-9,10-dione, FcMeAAQ = 1-(ferrocenylmethyl-amino)-anthraquinone, PTIO = 2-phenyl-4,4,5,5-tetramethylimidazoline-1-oxyl-3-oxide, H_2TPP = 5,10,15,20-tetraphenylporphyrin, Y-PVDF = Y-zeolite–poly (vinylidene fluoride) ion-selective membrane. – data not provided, * value estimated from data/figures.

Conclusion

A symmetric non-aqueous RFB employing PDI-TEMPO molecule as a bipolar redox-active material was designed, assembled and evaluated. PDI-TEMPO molecule was prepared via a simple, high yield, one-step synthesis method utilizing low cost and abundant precursors. The bipolar molecule demonstrated a good solubility of 1.3 M leading to a high energy density of 75.60 WhL^{-1}. CV measurements exhibited three redox processes with potential interval as high as 2.22 V. Battery testing demonstrated 100 consecutive charge and discharge cycles with a coulombic efficiency of over 90%. This work demonstrated better or comparable performance results versus the previously reported symmetric non-aqueous flow batteries. However, further investigation is required to address the stability/capacity loss issues to achieve high-performance parameters. This work introduces a new design of a bipolar organic molecule thus providing a basis for fabricating and developing multi-electron organic molecules for application in symmetric organic redox flow batteries.

Acknowledgement

The work described in this paper was fully supported by a grant from the Research Grants Council of the Hong Kong Special Administrative Region, China (Project No. T23-601/17-R). We also thank Biosciences Central Research Facility of HKUST for assistance in the mass spectrometry experiments. Research at Argonne National Laboratory was funded by the US Department of Energy (DOE) Vehicle Technologies Office under Contract No. DEAC02-

06CH11357. K.A. acknowledge the support of the U.S. China Clean Energy Research Center (CERC-CVC2).

References

[1] N.L. Panwar, S.C. Kaushik, S. Kothari, Role of renewable energy sources in environmental protection: A review, Renew. Sust. Energy Rev. 15 (2011) 1513-1524.

[2] D. Gielen, F. Boshell, D. Saygin, M.D. Bazilian, N. Wagner, R. Gorini, The role of renewable energy in the global energy transformation, Energy Strategy Rev. 24 (2019) 38-50.

[3] J.C. Stephens, Energy democracy: Redistributing power to the people through renewable transformation, Environment: Sci. Policy Sust. Dev. 61 (2019) 4-13.

[4] S. Jacobsson, V. Lauber, The politics and policy of energy system transformation—explaining the German diffusion of renewable energy technology, Energy Policy. 34 (2006) 256-276.

[5] D. Gielen, R. Gorini, N. Wagner, R. Leme, L. Gutierrez, G. Prakash, E. Asmelash, L. Janeiro, G. Gallina, G. Vale, Global energy transformation: a roadmap to 2050, (2019).

[6] Z. Yang, J. Zhang, M.C. Kintner-Meyer, X. Lu, D. Choi, J.P. Lemmon, J. Liu, Electrochemical energy storage for green grid, Chem. Rev. 111 (2011) 3577-3613.

[7] A. Manthiram, Y. Fu, Y. Su, In charge of the world: Electrochemical Energy Storage. J. Phys. Chem. Lett. (2013) 1295-1297.

[8] A.Z. Weber, M.M. Mench, J.P. Meyers, P.N. Ross, J.T. Gostick, Q. Liu, Redox flow batteries: a review, J. Appl. Electrochem. 41 (2011) 1137-1164.

[9] P. Alotto, M. Guarnieri, F. Moro, Redox flow batteries for the storage of renewable energy: A review, Renew. Sust. Energy Rev. 29 (2014) 325-335.

[10] J. Noack, N. Roznyatovskaya, T. Herr, P. Fischer, The chemistry of redox- flow batteries, Angew. Chem. Int. Ed. 54 (2015) 9776-9809.

[11] M. Bartolozzi, Development of redox flow batteries. A historical bibliography, J. Power Sources. 27 (1989) 219-234.

[12] R. Ye, D. Henkensmeier, S.J. Yoon, Z. Huang, D.K. Kim, Z. Chang, S. Kim, R. Chen, Redox flow batteries for energy storage: a technology review, J. Electrochem. Energy Convers. Storage. 15 (2018).

[13] J. Winsberg, T. Hagemann, T. Janoschka, M.D. Hager, U.S. Schubert, Redox- flow batteries: from metals to organic redox- active materials, Angew. Chem. Int. Ed. 56 (2017) 686-711.

[14] P. Leung, A.A. Shah, L. Sanz, C. Flox, J.R. Morante, Q. Xu, M.R. Mohamed, C.P. De León, F.C. Walsh, Recent developments in organic redox flow batteries: a critical review, J. Power Sources. 360 (2017) 243-283.

[15] X. Wei, W. Pan, W. Duan, A. Hollas, Z. Yang, B. Li, Z. Nie, J. Liu, D. Reed, W. Wang, Materials and systems for organic redox flow batteries: status and challenges, ACS Energy Lett. 2 (2017) 2187-2204.

[16] J. Luo, B. Hu, M. Hu, Y. Zhao, T.L. Liu, Status and prospects of organic redox flow batteries toward sustainable energy storage, ACS Energy Lett. 4 (2019) 2220-2240.

[17] V. Singh, S. Kim, J. Kang, H.R. Byon, Aqueous organic redox flow batteries, Nano Res. 12 (2019) 1988-2001.

[18] M. Li, Z. Rhodes, J.R. Cabrera-Pardo, S.D. Minteer, Recent advancements in rational design of non-aqueous organic redox flow batteries, Sustain. Energy & Fuels. 4 (2020) 4370-4389.

[19] X. Wei, W. Xu, J. Huang, L. Zhang, E. Walter, C. Lawrence, M. Vijayakumar, W.A. Henderson, T. Liu, L. Cosimbescu, Radical compatibility with nonaqueous electrolytes and its impact on an all- organic redox flow battery, Angew. Chem. Int. Ed. 54 (2015) 8684-8687.

[20] A. Ambrosi, R.D. Webster, 3D printing for aqueous and non-aqueous redox flow batteries, Curr. Opin. Electrochem. 20 (2020) 28-35.

[21] K.E. Rodby, M.L. Perry, F.R. Brushett, Assessing capacity loss remediation methods for asymmetric redox flow battery chemistries using levelized cost of storage, J. Power Sources. 506 (2021) 230085.

[22] A. Shrestha, K.H. Hendriks, M.S. Sigman, S.D. Minteer, M.S. Sanford, Realization of an Asymmetric Non- Aqueous Redox Flow Battery through Molecular Design to Minimize Active Species Crossover and Decomposition, Chem. Eur. J. 26 (2020) 5369-5373.

[23] C. Choi, S. Kim, R. Kim, Y. Choi, S. Kim, H. Jung, J.H. Yang, H. Kim, A review of vanadium electrolytes for vanadium redox flow batteries, Renew. Sust. Energy Rev. 69 (2017) 263-274.

[24] W. Duan, J. Huang, J.A. Kowalski, I.A. Shkrob, M. Vijayakumar, E. Walter, B. Pan, Z. Yang, J.D. Milshtein, B. Li, "Wine-Dark Sea" in an organic flow battery: storing negative charge in 2, 1, 3-benzothiadiazole radicals leads to improved cyclability, ACS Energy Lett. 2 (2017) 1156-1161.

[25] G.S. Nambafu, K. Siddharth, C. Zhang, T. Zhao, Q. Chen, K. Amine, M. Shao, An Organic Bifunctional Redox Active Material for Symmetric Aqueous Redox Flow Battery, Nano Energy. (2021) 106422.

[26] R.A. Potash, J.R. McKone, S. Conte, H.D. Abruña, On the benefits of a symmetric redox flow battery, J. Electrochem. Soc. 163 (2015) A338.

[27] P. Geysens, Y. Li, I. Vankelecom, J. Fransaer, K. Binnemans, Highly soluble 1, 4-diaminoanthraquinone derivative for nonaqueous symmetric redox flow batteries, ACS Sustain. Chem. Eng. 8 (2020) 3832-3843.

[28] G.D. Charlton, S.M. Barbon, J.B. Gilroy, C.A. Dyker, A bipolar verdazyl radical for a symmetric all-organic redox flow-type battery, J. Energy Chem. 34 (2019) 52-56.

[29] Y. Zhen, C. Zhang, J. Yuan, Y. Zhao, Y. Li, Ferrocene/anthraquinone based bi-redox molecule for symmetric nonaqueous redox flow battery, J. Power Sources. 480 (2020) 229132.

[30] G.S. Nambafu, M. Shao, Indigo Carmine/TEMPO Combined Bifunctional Molecule for a Total Organic Symmetric Aqueous Redox Flow Battery, ECS Meeting Abstracts. IOP Publishing. (2020) 495.

[31] T. Hagemann, J. Winsberg, B. Häupler, T. Janoschka, J.J. Gruber, A. Wild, U.S. Schubert, A bipolar nitronyl nitroxide small molecule for an all-organic symmetric redox-flow battery, NPG Asia Mater. 9 (2017) e340.

[32] W. Duan, R.S. Vemuri, J.D. Milshtein, S. Laramie, R.D. Dmello, J. Huang, L. Zhang, D. Hu, M. Vijayakumar, W. Wang, A symmetric organic-based nonaqueous redox flow battery and its state of charge diagnostics by FTIR, J. Mater. Chem. A. 4 (2016) 5448-5456.

[33] A. Korshunov, M.J. Milner, M. Grünebaum, A. Studer, M. Winter, I. Cekic-Laskovic, An oxo-verdazyl radical for a symmetrical non-aqueous redox flow battery, J. Mater. Chem. A. 8 (2020) 22280-22291.

[34] T. Ma, Z. Pan, L. Miao, C. Chen, M. Han, Z. Shang, J. Chen, Porphyrin- Based Symmetric Redox- Flow Batteries towards Cold- Climate Energy Storage, Angew. Chem. 130 (2018) 3212-3216.

[35] J. Friedl, M.A. Lebedeva, K. Porfyrakis, U. Stimming, T.W. Chamberlain, All-fullerene-based cells for nonaqueous redox flow batteries, J. Am. Chem. Soc. 140 (2018) 401-405.

[36] C.G. Armstrong, R.W. Hogue, K.E. Toghill, Application of the dianion croconate violet for symmetric organic non-aqueous redox flow battery electrolytes, J. Power Sources. 440 (2019) 227037.

[37] J. Gawroński, M. Brzostowska, K. Gawrońska, J. Koput, U. Rychlewska, P. Skowronek, B. Nordén, Novel Chiral Pyromellitdiimide (1, 2, 4, 5- Benzenetetracarboxydiimide) Dimers and Trimers: Exploring Their Structure, Electronic Transitions, and Exciton Coupling, Chem. Eur. J. 8 (2002) 2484-2494.

[38] D.J. Kim, K.R. Hermann, A. Prokofjevs, M.T. Otley, C. Pezzato, M. Owczarek, J.F. Stoddart, Redox-active macrocycles for organic rechargeable batteries, J. Am. Chem. Soc. 139 (2017) 6635-6643.

[39] G. Nambafu, M. Shao, Bipolar Diimide Based Molecule for Nonaqueous Symmetric Redox Flow Battery, ECS Meeting Abstracts. IOP Publishing (2021) 228.

[40] T. Abdinejad, M.R. Zamanloo, T. Alizadeh, N.O. Mahmoodi, S.R. Pouran, Photochromic and Electrochromic Diimide Synthesized Simply from Inexpensive Compounds: A Multidisciplinary Experiment for Undergraduate Students, J. Chem. Educ. 95 (2018) 1642-1647.

[41] A.T. Celebi, S.H. Jamali, A. Bardow, T.J. Vlugt, O.A. Moultos, Finite-size effects of diffusion coefficients computed from molecular dynamics: a review of what we have learned so far, Mol. Simul. (2020) 1-15.

[42] T.C. Chan, H.T. Li, K.Y. Li, Effects of shapes of solute molecules on diffusion: A study of dependences on solute size, solvent, and temperature, J. Phys. Chem. B. 119 (2015) 15718-15728.

[43] A.J. Bard, L.R. Faulkner, Fundamentals and applications, Electrochemical methods. 2 (2001) 580-632.

[44] A.M. Kosswattaarachchi, T.R. Cook, Concentration-dependent charge-discharge characteristics of non-aqueous redox flow battery electrolyte combinations, Electrochim. Acta, 261 (2018) 296-306.

[45] X. Wang, A. Lashgari, J. Chai, A membrane-free, aqueous/nonaqueous hybrid redox flow battery. Energy Stor. Mater. (2021).

[46] K. Gong, Q. Fang, S. Gu, S.F.Y. Li, Y. Yan, Nonaqueous redox-flow batteries: organic solvents, supporting electrolytes, and redox pairs, Energy Environ. Sci. 8 (2015) 3515-3530.

[47] A.A. Shinkle, T.J. Pomaville, A.E. Sleightholme, L.T. Thompson, C.W. Monroe, Solvents and supporting electrolytes for vanadium acetylacetonate flow batteries, J. Power Sources, 248 (2014) 1299-1305.

[48] Y. Huang, S. Gu, Y. Yan, S.F.Y. Li, Nonaqueous redox-flow batteries: features, challenges, and prospects. Curr. Opin. Chem. Eng. 8 (2015) 105-113.

[49] X. Wei, W. Duan, J. Huang, L. Zhang, B. Li, D. Reed, W. Xu, V. Sprenkle, W. Wang, A high-current, stable nonaqueous organic redox flow battery, ACS Energy Letters. 1 (2016) 705-711.

[50] S. Er, C. Suh, M.P. Marshak, A. Aspuru-Guzik, Computational design of molecules for an all-quinone redox flow battery, Chem. Sci. 6 (2015) 885-893.

[51] Y. Ding, C. Zhang, L. Zhang, Y. Zhou, G. Yu, Molecular engineering of organic electroactive materials for redox flow batteries, Chem. Soc. Rev. 47 (2018) 69-103.

[52] F.R. Brushett, M.J. Aziz, K.E. Rodby, On lifetime and cost of redox-active organics for aqueous flow batteries, ACS Energy Lett. 5 (2020) 879-884.

[53] P.S. Engel, W.K. Lee, G.E. Marschke, H.J. Shine, The reactions of 1-adamantyl radicals with acetonitrile and their bearing on the oxidative decomposition of 1, 1'-azoadamantane, J. Org. Chem. 52 (1987) 2813-2817.

[54] X. Wei, W. Xu, J. Huang, L. Zhang, E. Walter, C. Lawrence, M. Vijayakumar, W.A. Henderson, T. Liu, L. Cosimbescu, Radical compatibility with nonaqueous electrolytes and its impact on an all- organic redox flow battery, Angew. Chem. Int. Ed. 54 (2015) 8684-8687.

[55] V.S. Bryantsev, V. Giordani, W. Walker, M. Blanco, S. Zecevic, K. Sasaki, J. Uddin, D. Addison, G.V. Chase, Predicting solvent stability in aprotic electrolyte Li–air batteries: nucleophilic substitution by the superoxide anion radical (O2•–), J. Phys. Chem. A. 115 (2011) 12399-12409.

[56] M. Li, J. Case, S.D. Minteer, Bipolar Redox- Active Molecules in Non- Aqueous Organic Redox Flow Batteries: Status and Challenges, ChemElectroChem. 8 (2021) 1215-1232.